Research Square

Preprints are preliminary reports that have not undergone peer review.
They should not be considered conclusive, used to inform clinical practice,
or referenced by the media as validated information.

CFD-DPM Sensitivity Analysis of Particle and Conveying Parameters on Pressure Drop in Dilute-Phase Pneumatic Conveying of Teff Grain

Lemi Demissie Boset

lemid@du.edu.et

Dilla University

Research Article

Keywords: CFD-DPM, dilute-phase pneumatic conveying, particle properties, pressure drop, sensitivity analysis, teff grain

Posted Date: September 2nd, 2026

DOI: https://doi.org/10.21203/rs.3.rs-10706988/v1

License: This work is licensed under a Creative Commons Attribution 4.0 International License.
Read Full License

Additional Declarations: No competing interests reported.

CFD-DPM Sensitivity Analysis of Particle and Conveying Parameters on Pressure Drop in Dilute-Phase Pneumatic Conveying of Teff Grain

Lemi Demissie Boset

Department of Mechanical Engineering, College of Engineering, Dilla University, Dilla, Ethiopia

Corresponding author email: lemid@du.edu.et

Abstract

Efficient pneumatic conveying of fine agricultural grains requires an understanding of how conveying conditions and particle properties affect pressure loss. This study presents a CFD-DPM sensitivity analysis of pressure drop in dilute-phase pneumatic conveying of teff grain, considering air velocity, pipe diameter, particle sphericity, particle density, and particle diameter. A total of 243 CFD-DPM simulation cases were systematically evaluated across representative parameter ranges. Pressure-drop results were analyzed using marginal means, variability measures, and percentage changes to determine the relative influence of the investigated variables. Predicted pressure drop ranged from 43.67 to 480.03 Pa, with an overall mean of 158.58 Pa. Among the system parameters, air velocity had the greatest influence, with mean pressure drop increasing from 108.04 Pa at 16 m/s to 209.26 Pa at 24 m/s, corresponding to a 93.7% increase. Increasing pipe diameter from 46 to 102 mm reduced mean pressure drop by 54.9%. Among the particle properties, sphericity showed the greatest effect, with variation from 0.67 to 0.70 associated with a 50.3% reduction in mean pressure drop. Variations in particle density from 1120 to 1381 kg/m³ and particle diameter from 0.68 to 0.72 mm increased mean pressure drop by 17.9% and 16.6%, respectively. The relative influence of the investigated variables followed the order air velocity > pipe diameter ≈ sphericity > density > particle diameter. Overall, the results demonstrate that system parameters have a greater influence on pressure loss than particle properties within the investigated ranges. The findings provide quantitative engineering guidance for selecting conveying velocity and pipe diameter and for incorporating particle characteristics into pressure-drop prediction. The results support the design and optimization of dilute-phase pneumatic conveying systems for teff grain and provide a foundation for evaluating similar dry fine bulk materials.

Keywords: CFD-DPM; dilute-phase pneumatic conveying; particle properties; pressure drop; sensitivity analysis; teff grain

1. Introduction

Pneumatic conveying systems serve as an essential cornerstone in bulk solids processing, playing a central role across agricultural processing, food manufacturing, pharmaceuticals, energy production, and chemical engineering [1]. The broad industrial adoption of pneumatic transport stems from its distinct operational advantages, including flexible routing across complex layouts, a minimal physical footprint, complete pipeline enclosure to eliminate dust emissions and contamination, and high automation potential for continuous material transfer [1, 27]. Within post-harvest agricultural engineering, efficient mechanical conveying is critical for moving cleaned grains between storage silos, drying units, cleaning separators, and milling machinery [1, 26].

Among global cereal crops, teff (*Eragrostis tef*) holds supreme socio-economic, agricultural, and nutritional importance, particularly in East Africa where it forms a staple food source [1, 42]. Teff is widely praised for its resilience to variable climates, high nutritional density, gluten-free property, and rich mineral profile [1, 42]. However, handling teff presents severe mechanical challenges compared to major cereal grains like corn, wheat, or rice [1, 5, 42]. With an individual grain length ranging between 0.6 and 1.2 mm and an average thousand-grain weight of only 0.25 to 0.40 grams, teff is among the smallest cultivated food grains in the world [1, 42]. Traditional post-harvest transport and handling practices for teff frequently suffer from high manual labor requirements, operational inefficiencies, and physical loss rates reaching 16% to over 30% [1, 3, 5]. Implementing automated, energy-efficient dilute-phase pneumatic conveying systems offers a viable technical pathway to minimize post-harvest losses, protect grain quality, and streamline processing throughput [3, 5, 27]. Dilute-phase transport characterized by high carrier gas velocities ($v > 15$ m/s), low solid volumetric fractions, and fully suspended particle motion is uniquely suited for fine agricultural seeds like teff [3, 5, 19, 27].

A fundamental requirement in designing, sizing, and operating pneumatic conveying pipelines is the accurate prediction and minimization of system static pressure drop (ΔP) [3, 5, 27, 33]. Total pressure loss directly dictates the fan or blower power requirements, directly driving capital equipment costs, operational energy consumption, and overall flow stability [6, 19, 27, 39]. In dilute-phase gas-solid flows, total pressure drop is a complex composite response governed by gas-wall friction, particle acceleration forces, particle-wall collisions, gravitational lift drag, and particle-particle momentum exchanges [7, 18, 19, 22]. Engineers historically relied on empirical correlations and simplified semi-analytical models to estimate pneumatic pressure losses [7, 10, 33, 35, 38]. While these classical relationships perform adequately for uniform spherical beads or large coarse grains, they frequently fail when applied to small, non-spherical, fine agricultural particles like teff [1, 5, 11, 12, 42]. Teff grains exhibit significant departures from spherical geometry (ϕ= 0.67-0.70), along with micro-scale variations in grain density (ρ) and geometric size (d_p) across different genetic cultivars [1, 3, 5, 42].

To overcome these analytical limitations, Computational Fluid Dynamics coupled with the Discrete Phase Model (CFD-DPM) has emerged as an advanced Eulerian-Lagrangian numerical framework [5, 9, 14, 21, 36]. In CFD-DPM, the continuous carrier air phase is solved using Eulerian Navier-Stokes equations, while individual grain trajectories are tracked explicitly in a Lagrangian reference frame by balancing forces including aerodynamic drag, gravity, pressure gradients, and non-spherical shape coefficients [9, 11, 12, 17, 36, 37]. Two-way momentum coupling ensures that local fluid-particle momentum transfer is accurately captured, providing high-resolution prediction of pipe pressure fields [9, 16, 22, 34]. Despite expanding research on CFD-DPM modeling for major agricultural grains, comprehensive parametric sensitivity evaluations focusing on fine, highly non-spherical bulk seeds remain scarce [3, 5, 21, 36]. Existing literature frequently isolates single operational parameters (e.g., velocity or pipe size) while assuming fixed, idealized particle morphology [21, 36]. However, real-world conveying performance is governed by a simultaneous interplay between operational variables (air velocity, pipe diameter) and intrinsic grain properties (sphericity, density, cultivar-dependent size) [3, 5, 19, 27].

To bridge this research gap, this study conducts a comprehensive CFD-DPM numerical sensitivity analysis of static pressure drop (ΔP) in dilute-phase horizontal pneumatic conveying of teff grain [3]. Five primary design factors are systematically evaluated across a complete 3^5 full factorial

parameter space comprising 243 simulation cases [3]. These factors comprise pipe diameter (D evaluated at 46, 71, and 102 mm), conveying air velocity (v evaluated at 16, 20, and 24 m/s), particle sphericity (ϕ evaluated at 0.67, 0.68, and 0.70), particle density (ρ evaluated at 1120, 1284, and 1381 kg/m³), and representative particle diameter (d_p evaluated at 0.68, 0.70, and 0.72 mm, reflecting three Ethiopian teff cultivars: Felagot, Dagim, and Bishoftu) [3]. Through marginal mean evaluations, dispersion metrics, and relative percentage changes across the 243 cases, this study isolates individual parameter effects, provides engineering sensitivity rankings, and quantifies key parameter interaction trends [3]. The findings supply practical design criteria for optimizing energy-efficient pneumatic transport systems tailored specifically for teff bulk handling [3, 5].

2. Materials and Methods

2.1 Teff Grain

Three Ethiopian teff (Eragrostis tef) varieties Felagot (DZ-Cr-442RIL77C), Dagim (DZ-Cr-438RIL91A), and Bishoftu (DZ-Cr-497RIL133) were selected to represent variation in genetic background and physical grain characteristics. Grain samples were obtained from National Teff Improvement Program at the Debre Zeit Agricultural Research Center (DZARC), the primary teff research center in Ethiopia operating under the Ethiopian Institute of Agricultural Research (EIAR) [4]. Necessary permissions and material access approvals were obtained from the breeding program at DZARC/EIAR prior to sample collection. The varieties were sourced from this established agricultural research and breeding program and used to characterize the physical and particle properties relevant to pneumatic conveying. All plant materials were collected and handled solely for this study in full compliance with institutional, local, and national guidelines.

Before characterization, samples were manually cleaned to remove foreign materials, broken kernels, and contaminants [4]. Cleaned grains were maintained under laboratory ambient conditions until testing [4]. Using three cultivars allowed particle diameter and associated characteristics to be represented within a range relevant to Ethiopian teff grains rather than treating teff as a single geometrically uniform material [1,4,42].

2.3 Moisture Content Determination

The moisture content of the grain samples was determined before physical characterization using the forced-air oven method described in ASAE S352.3 (ASAE Standards, 1994). Representative grain samples were weighed before drying using electronic balances with capacities and resolutions of 0-3 kg / 0.1 g and 0–250 g / 0.01 mg, respectively [27]. Samples were dried at 100-105°C until a constant mass was reached [27]. Moisture content on a wet basis (MC) was calculated as:

$$MC = \frac{(w - d)}{w} \times 100 \quad (1)$$

Where MC is moisture content on a wet basis (%), w is initial wet mass (g), and d is final dry mass (g) [27].

2.4 Particle Dimensional Characterization

Particle dimensions were determined for 20 kernels from each cultivar using high-resolution two-dimensional scanning electron microscopy (SEM) images. Image analysis was performed to measure the principal dimensions: grain length (L) and width (W). Grain thickness (T) was

estimated using established dimensional relationships for teff grains (Zewdu and Solomon, 2007; Abewa et al., 2019).The arithmetic mean diameter (Da) was calculated as [4]:

$$D_g = \sqrt[3]{W \times T \times L} \quad (2)$$

The geometric mean diameter (Dg) was determined from:

$$D_a = \frac{W + T + L}{3} \quad (3)$$

Where L, W, and T are grain length, width, and thickness in millimeters, respectively [4]. Geometric mean diameter (D_g) was selected as the representative particle diameter (d_p) for the numerical model because it incorporates all three principal dimensions and provides a convenient equivalent diameter for representing non-spherical particles in the CFD-DPM model [4,5, 17].

2.5 Particle Density

Particle density (ρp) was included as a numerical sensitivity parameter with three evaluated levels: 1120 kg/m³, 1284 kg/m³, and 1381 kg/m³. The intermediate value of 1284 kg/m³ served as the baseline/reference condition in the CFD-DPM analysis. Density values were directly assigned to discrete phase material properties in the CFD-DPM model, keeping all other parameters constant [5].

2.6 Particle Sphericity

To account for non-spherical particle geometry in gas-particle momentum exchange, particle sphericity (ϕ) was explicitly introduced. The three investigated levels were 0.67, 0.68, and 0.70. For a particle with volume V_p and surface area A_p, sphericity is defined as [17-18]:

$$\phi = \frac{\Pi^{\frac{1}{3}} \cdot (6 \cdot V_p)^{\frac{2}{3}}}{A_p} \quad (4)$$

A value of ϕ = 1 represents a perfect sphere, whereas lower values indicate increasing deviation from spherical geometry.

2.7 Representative Particle Diameter and Teff Variety

The representative particle diameters (d_p) corresponding to the three teff cultivars were defined as: Felagot: dp = 0.68 mm, Dagim: d_p = 0.70 mm and Bishoftu: d_p = 0.72 mm. Particle diameter was treated as a continuous physical factor rather than using cultivar identity as a discrete qualitative variable, providing physically meaningful particle-size levels for sensitivity evaluation [3-50].

The study employed a numerical factorial approach to investigate the sensitivity of pressure drop in dilute-phase pneumatic conveying of teff grain to selected particle and conveying parameters [3,5]. Five factors were considered: pipe diameter (D), conveying-air velocity (v), particle sphericity (ϕ), particle density (ρ_p), and representative particle diameter (d_p) [3]. Each factor was assigned three levels, resulting in a complete 3^5 factorial parameter space containing 243 combinations [3].

The investigated levels were selected to represent the range of particle and conveying characteristics relevant to the pneumatic transport of teff grain [1,3,5, 42]. The five factors and their levels are presented in Table 1.

Table 1: Experimental factors and levels for the numerical sensitivity study.

Parameter	Symbol	Level 1	Level 2	Level 3
Pipe diameter (mm)	D	46	71	102

Air velocity (m/s)	v	16	20	24
Particle sphericity	ϕ	0.67	0.68	0.70
Particle density (kg/m^3)	ρ_p	1120	1284	1381
Particle diameter (mm)	d_p	0.68	0.70	0.72

The analysis was designed to quantify both the overall sensitivity of pressure drop to individual parameters and the changes in response observed under selected combinations of conveying conditions [3]. Marginal mean pressure drops were calculated for each parameter by averaging the predicted pressure-drop values over all combinations of the remaining parameters.

2.8 Numerical Parameter Space and Factorial Design

A complete 3^5 full factorial design yielded the total number of numerical runs (N) [3]:

$$N = 3^5 = 243 \tag{5}$$

For each parameter level i, the marginal mean pressure drop ($\bar{P}_i$) was calculated across $n_i = 81$ conditions (3^4 combinations of remaining factors) using [3]:

$$\bar{P}_i = \frac{1}{n_i}\sum_{j=1}^{n} P_{ij} \tag{6}$$

Where P_{ij} is the predicted pressure drop obtained for the j-th combination at level i.

2.9 CFD-DPM Model Development

The pneumatic conveying system was modeled using ANSYS SpaceClaim 2024 R1 for geometry construction and ANSYS Fluent 2024 R1 for CFD and discrete phase calculations. The computational domain represented a straight circular horizontal conveying pipe under dilute-phase conditions [5,6].

The continuous gas phase was treated using an Eulerian formulation, while teff grains were tracked as a discrete Lagrangian phase via the Discrete Phase Model (DPM) [5, 19, 21]. Two-way momentum coupling was enabled between the gas and particle phases. Where required, the Rosin-Rammler distribution was used to represent particle size variations [19].

2.10 Governing Equations

Gas Phase Conservation Equations

For an incompressible continuous gas phase, mass conservation (continuity equation) is given by [19,30]:

$$\Delta \cdot \left(\rho_g \cdot u\right) = 0 \tag{7}$$

Where ρ_g is the gas density and u is the gas velocity vector [19].

The momentum conservation equation for the gas phase is expressed as [19, 22, 30]:

$$\nabla \cdot \left(\rho_g \cdot u \cdot u\right) = \nabla_p + \nabla \cdot \tau + S_m \tag{8}$$

Where p is static pressure, τ is the viscous stress tensor, and S_m is the momentum source term accounting for two-way phase interactions with DPM particles [19, 22].

Discrete Particle Lagrangian Equation of Motion

The trajectory of individual discrete teff particles was computed by balancing forces in a Lagrangian reference frame [19, 21, 25]:

$$m_p \cdot \frac{du_p}{dt} = F_D + F_G + F_{other} \quad (9)$$

Where m_p is particle mass, up is particle velocity vector, F_D is aerodynamic drag force, F_G is gravitational force ($m_p \cdot g$), and Fother represents additional forces (e.g., virtual mass, pressure gradient forces). The drag force F_D is defined as [17, 18, 23]:

$$F_D = \frac{1}{2} \cdot C_D \cdot \rho_g \cdot A_p \cdot \left|u - u_p\right| \cdot \left(u - u_p\right) \quad (10)$$

Where C_D is the drag coefficient, dependent on particle Reynolds number (R_{ep}) and sphericity (ϕ).

2.11 Turbulence and Wall Treatment

Turbulent flow within the pipe was modeled using the k–ϵ turbulence model formulation. Enhanced wall treatment/standard wall functions were applied based on the near-wall boundary layer conditions. The target wall y^+ coordinate was maintained within the log-law domain ($30 < y^+ < 300$), where y^+ is defined as [19]:

$$y^+ < \frac{u_* \cdot y}{\nu} \quad (11)$$

In which u_* is friction velocity, y is distance to the nearest wall, and v is kinematic viscosity.

2.12 Computational Mesh and Independence Assessment

Unstructured computational meshes were generated with element sizes ranging from 3 mm to 8 mm. Mesh independence was confirmed when successive mesh refinements produced negligible changes (< 1%) in predicted pressure drop under baseline operating conditions prior to execution of the 243 factorial runs [5,6].

2.13 Boundary Conditions and Solution Procedure

At the pipe inlet, continuous air was introduced with uniform velocity profiles (v = 16, 20, 24 m/s). A no-slip boundary condition was prescribed at the pipe walls. Particles were injected uniformly at the inlet matching gas velocities. Iterative calculations were conducted using pressure-velocity coupling schemes until normalized residuals dropped below 10^{-4} for momentum and turbulence equations, and pressure drop stabilized [5,19].

2.14 Pressure-Drop Calculation

The net total pressure drop (ΔP) across the pipe length was computed as [2, 7]:

$$\Delta P = P_{in} + P_{out} \quad (12)$$

Where P_{in} and P_{out} are static pressures measured at reference inlet and outlet cross-sections.

The dimensionless pressure-drop loss coefficient (K) was evaluated as [2, 7,15]:

$$K = \frac{\Delta P}{\frac{1}{2} \cdot \rho_g \cdot \upsilon^2} \quad (13)$$

Where ρ_g is gas density and υ is conveying-air velocity.

2.15 Sensitivity Analysis Formulas

Relative percentage change in marginal mean pressure drop (%ΔP) from the minimum level baseline ($\bar{P}_{min}$) was computed using [3]:

$$\%\Delta P = \frac{\bar{P}_i - \bar{P}_{\min}}{\bar{P}_{\min}} \times 100 \tag{14}$$

The sample standard deviation (S_D) quantifying response dispersion at each parameter level was calculated as [3]:

$$S_D = \sqrt{\frac{1}{n_i - 1}\sum_{j=1}^{n}(P_{ij} - \bar{P}_i)^2} \tag{15}$$

The coefficient of variation (C_V) was evaluated as:

$$CV = \frac{SD}{\bar{P}_i} \times 100 \tag{16}$$

Parameters were ranked by engineering magnitude based on maximum relative changes in marginal means.

2.16 Data Analysis and Presentation

The complete factorial dataset was evaluated through marginal means (overall sensitivity) and conditional means (identifying factor interaction trends). Line graphs and normalized sensitivity charts were generated to compare responses across all five investigated parameters [3].

3. Results and Discussions

3.1 CFD-DPM Simulation Results

A numerical sensitivity study was carried out to evaluate the influence of key operating and material parameters on the pressure and velocity fields developed during dilute-phase pneumatic conveying. Five factors, namely pipe diameter, air velocity, particle sphericity, particle density, and particle diameter, were each varied across three levels, giving the experimental design summarised in Table 1. In all cases the pipe length was fixed at L = 1000 mm and the solids mass flow rate was held constant at m_s = 0.1 kg/s. Simulations were run for the diameter, sphericity, density, and particle-size levels listed in Table 1, and the static pressure and air velocity contour fields were extracted along the pipe centreline plane for post-processing, as presented in Fig. 1.

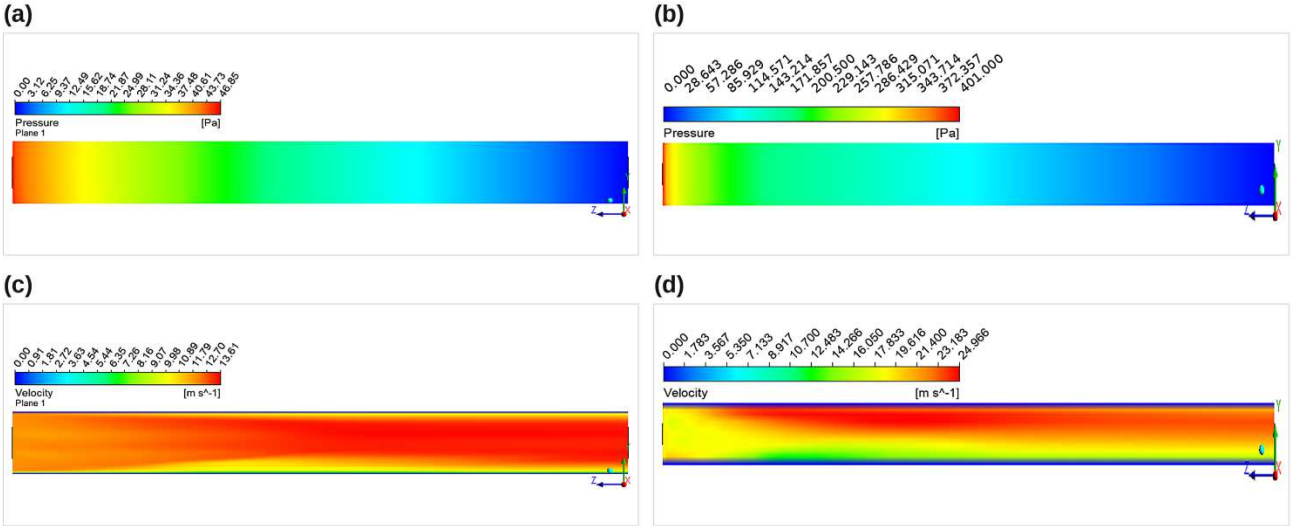

Fig. 1. Contours of (a, b) static pressure and (c, d) air velocity along the pipe cross-section at air velocities of (a, c) v = 12 m/s and (b, d) v = 24 m/s, for d_p= 0.72mm, D= 46mm, ϕ=0.70, ρ_p = 1381 kg/m³ and L = 1000 mm.

Figure 1 shows a nearly linear decrease in static pressure along the pipe, with a much greater pressure drop at 24 m/s (up to 401 Pa) than at 16 m/s (up to 47 Pa), consistent with the quadratic dependence of pressure loss on air velocity. The velocity contours show flow development from a low-velocity wall region to a more uniform downstream profile, with faster development and a higher, sharper core velocity at 24 m/s.

The following figures present line graphs illustrating the effects of five key parameters pipe diameter, air conveying velocity, particle sphericity, particle density, and particle diameter (teff variety) on the predicted pressure drop (ΔP) in dilute-phase pneumatic conveying of teff grain. Each graph plots mean ΔP (Pa) across the relevant parameter levels, averaged across all remaining variables, to isolate the effect of each factor. A total of 243 simulation cases were analyzed.

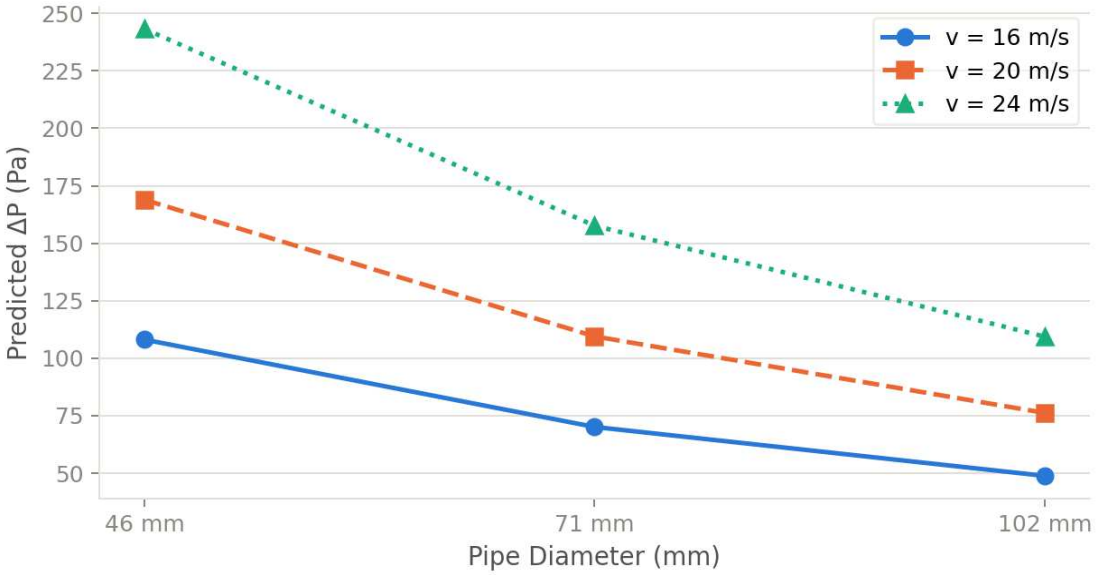

Fig. 2. Effect of Pipe Diameter and Air Velocity on Mean Predicted ΔP

Figure 2 illustrates the combined influence of pipe diameter and air conveying velocity on mean predicted pressure drop. A consistent inverse relationship between pipe diameter and ΔP is observed across all three air velocity levels. At v = 16 m/s, ΔP decreases from 108.04 Pa at D = 46 mm to 48.76 Pa at D = 102 mm, representing a reduction of 54.9%. Similarly, at v = 24 m/s, pressure drop declines from 243.26 Pa to 109.36 Pa over the same pipe diameter range. The results confirm that pipe diameter is a dominant design variable for minimizing energy loss in dilute-phase pneumatic conveying of teff grain.

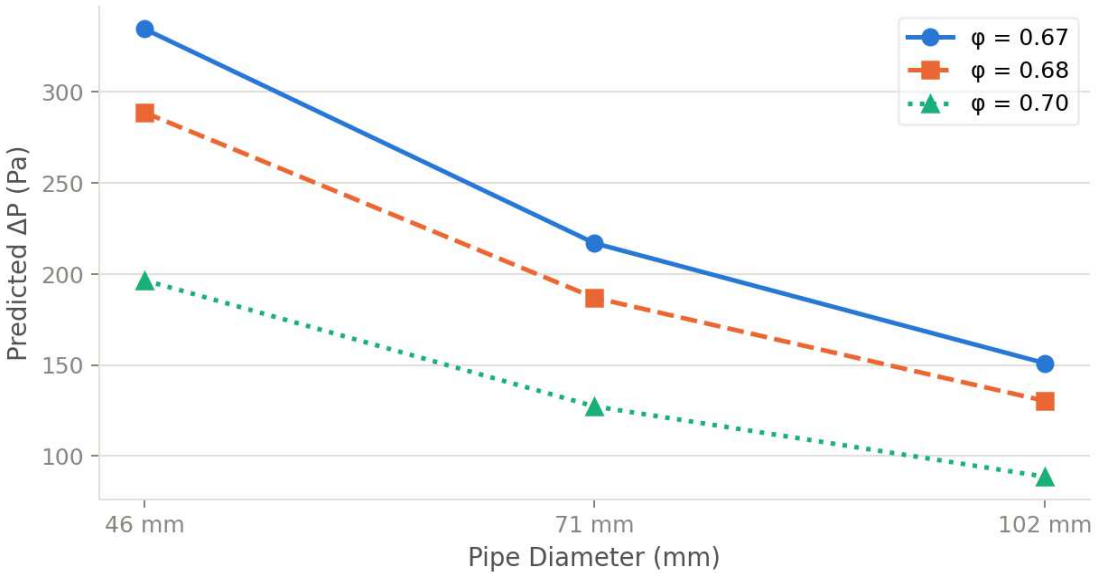

Fig. 3. Effect of Sphericity on Mean Predicted ΔP Across Pipe Diameters

Figure 3 demonstrates that particle sphericity has the most pronounced influence on pressure drop among all parameters investigated. At D = 46 mm, increasing sphericity from φ = 0.67 to φ = 0.70 reduces ΔP from 334.68 Pa to 196.54 Pa a decrease of 41.2%. At D = 102 mm, the same sphericity increase reduces ΔP from 150.99 Pa to 88.58 Pa (−41.3%). The near-parallel nature of the three curves across all pipe diameters indicates that sphericity exerts an independent, additive effect that does not strongly interact with pipe size. This finding has significant practical implications: teff varieties or post-harvest treatments that produce more spherical grains will substantially reduce conveying energy requirements.

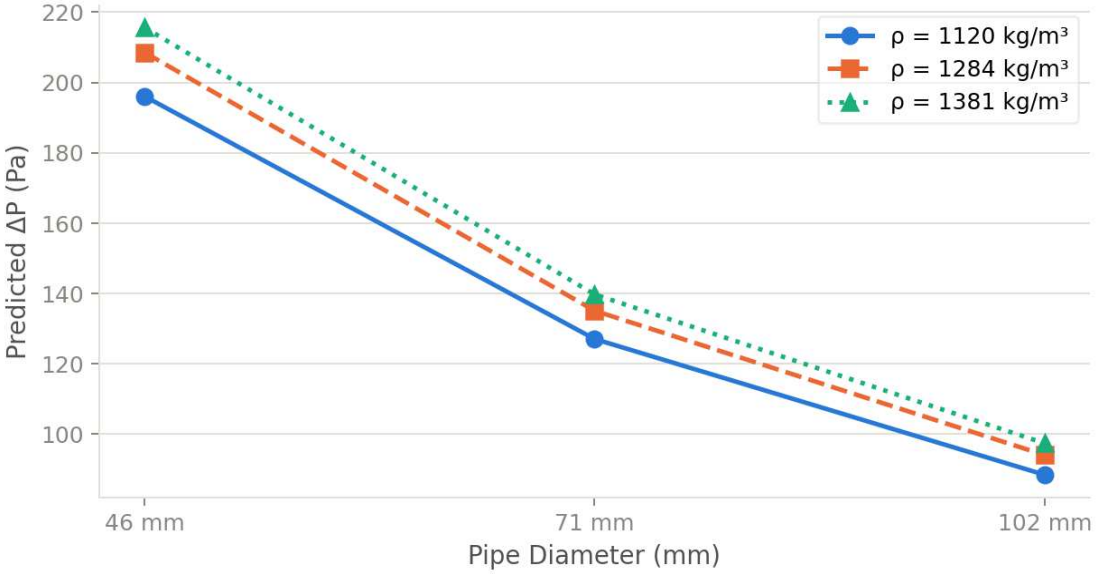

Fig. 4. Effect of Particle Density on Mean Predicted ΔP Across Pipe Diameters

Figure 4 shows the effect of particle density on predicted pressure drop across the three pipe diameters. As density increases from 1120 to 1381 kg/m³, mean ΔP increases consistently at each pipe size by approximately 9.98% at D = 46 mm, 10.0% at D = 71 mm, and 10.1% at D = 102 mm.

The three curves follow closely parallel trajectories, confirming that particle density has a moderate and uniform influence on ΔP that does not strongly interact with pipe geometry. Although the absolute magnitude of the density effect is smaller than those of sphericity and air velocity, it remains practically significant when selecting conveying conditions for different teff grain varieties.

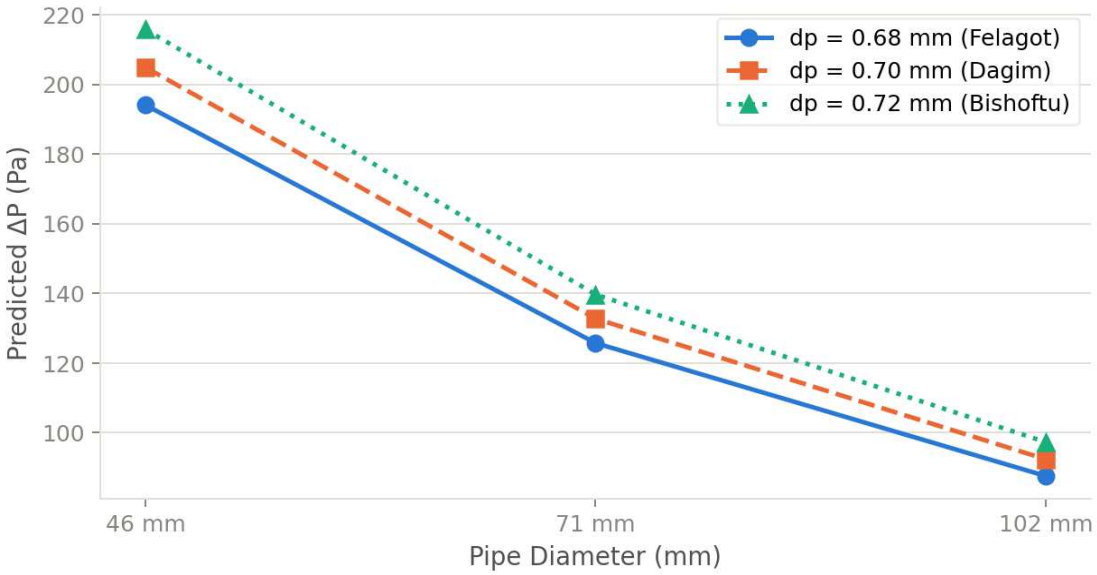

Fig. 5. Effect of Particle Diameter (Teff Variety) on Mean Predicted ΔP

Figure 5 presents the influence of particle diameter, corresponding to three teff grain varieties, on predicted pressure drop. Felagot (d_p = 0.68 mm), Dagim (d_p = 0.70 mm), and Bishoftu (d_p = 0.72 mm) exhibit progressively higher pressure drops at each pipe diameter. At D = 46 mm, ΔP increases from 194.05 Pa (Felagot) to 215.76 Pa (Bishoftu), a difference of 11.2%. The narrow spacing between the three curves across all pipe diameters confirms that particle diameter has the least influence among all parameters studied. Nevertheless, variety-specific differences are non-trivial and should be accounted for in system design when conveying different teff varieties in the same pipeline.

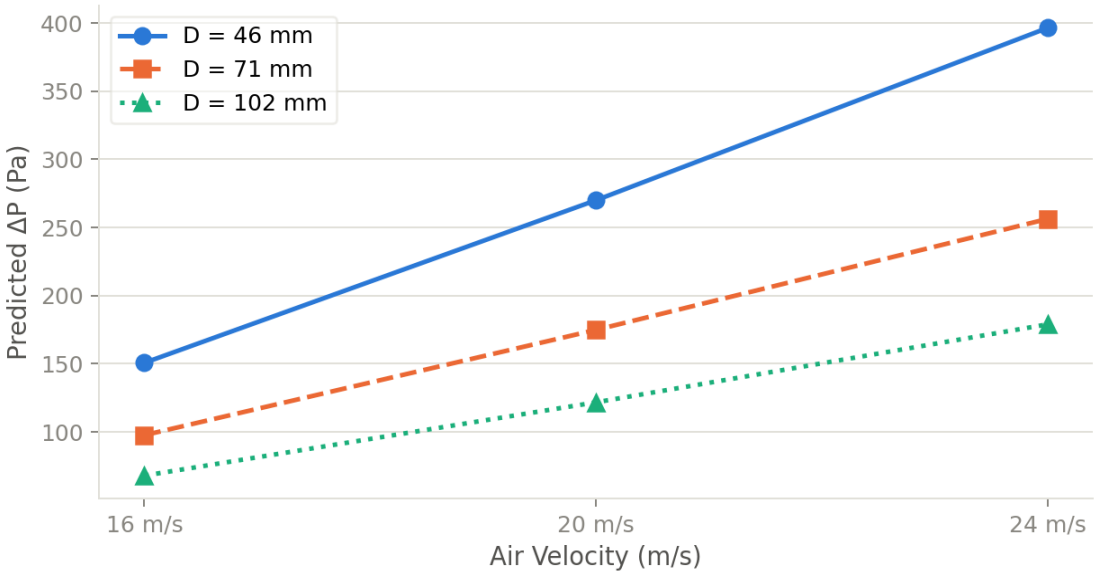

Fig. 6. Effect of Air Velocity on Mean Predicted ΔP by Pipe Diameter

Figure 6 illustrates how air conveying velocity influences predicted pressure drop across the three pipe diameters. All three pipe sizes show a strong positive relationship between air velocity and ΔP. For D = 46 mm, pressure drop increases from 150.69 Pa at v = 16 m/s to 396.35 Pa at v = 24 m/s a rise of 163%. For D = 102 mm, the increase over the same velocity range is 68.00 Pa to 178.95 Pa (+163%). The diverging trend of the curves as velocity increases indicates a significant pipe diameter × velocity interaction: higher velocities amplify the pressure difference between small and large pipes, making pipe diameter selection increasingly critical at higher conveying speeds.

Table 2. Statistical Analysis of Predicted Pressure Drop by Key Parameters

Parameter	Level	N	Mean ΔP (Pa)	Std Dev (Pa)	Min (Pa)	Max (Pa)	CV (%)	% Change
Pipe Diameter (mm)	46	81	227.37	96.12	96.84	480.03	42.3	baseline
	71	81	147.36	62.42	62.74	311.00	42.4	−35.2%
	102	81	102.62	43.39	43.67	216.48	42.3	−54.9%
Air Velocity (m/s)	16	81	108.04	45.11	43.67	213.34	41.8	baseline
	20	81	168.89	70.50	68.24	333.35	41.7	+56.3%
	24	81	209.26	87.43	98.26	480.03	41.8	+93.7%
Sphericity (–)	0.67	81	206.07	91.14	106.89	480.03	44.2	baseline
	0.68	81	177.72	78.61	92.17	413.93	44.2	−13.8%
	0.70	81	102.38	45.29	43.67	281.75	44.2	−50.3%
Particle Density (kg/m³)	1120	81	149.93	83.07	43.67	435.76	55.4	baseline
	1284	81	159.52	88.37	46.46	463.57	55.4	+6.4%
	1381	81	176.73	93.59	48.11	480.03	52.9	+17.9%
Particle Diameter (mm)	0.68	81	146.26	84.01	43.67	408.91	57.4	baseline
	0.70	81	158.96	88.25	45.12	444.47	55.5	+8.7%
	0.72	81	170.51	93.16	51.27	480.03	54.6	+16.6%
Overall	—	243	158.58	88.51	43.67	480.03	55.8	—

CV = Coefficient of Variation. % Change calculated relative to the lowest level of each parameter

Table 2 summarizes the predicted pressure-drop response across the 243 simulation cases. Pipe diameter and air velocity exhibited the largest effects among the investigated conveying parameters. Increasing pipe diameter from 46 to 102 mm reduced the mean predicted pressure

drop from 227.37 to 102.62 Pa, corresponding to a 54.9% reduction. In contrast, increasing air velocity from 16 to 24 m/s increased mean pressure drop from 108.04 to 209.26 Pa, representing a 93.7% increase. Particle sphericity also showed a substantial effect, with an increase from 0.67 to 0.70 reducing mean ΔP by 50.3%. The effects of particle density and particle diameter were comparatively smaller, with increases from their respective minimum to maximum levels producing 17.9% and 16.6% increases in mean pressure drop. Across all 243 cases, ΔP ranged from 43.67 to 480.03 Pa, with an overall mean of 158.58 Pa and a coefficient of variation of 55.8%. These results indicate that conveying velocity is the most influential parameter based on the observed marginal mean change, followed by pipe diameter and particle sphericity, whereas density and particle diameter exert relatively smaller effects within the investigated ranges.

4. Conclusion

The study numerically investigated the effects of system parameters and particle properties on pressure drop (ΔP) during dilute-phase pneumatic conveying of teff grain using 243 simulation cases. The investigated system parameters were air velocity and pipe diameter, while the particle properties included sphericity, density, and diameter. The predicted pressure drop ranged from 43.67 to 480.03 Pa, with a mean of 158.58 Pa and a coefficient of variation of 55.8%, indicating considerable variation across the investigated conditions.

Among the system parameters, air velocity and pipe diameter exerted the greatest influence on pressure drop. Increasing air velocity from 16 to 24 m/s increased mean ΔP by 93.7%, whereas increasing pipe diameter from 46 to 102 mm reduced mean ΔP by 54.9%. These results demonstrate that system parameters have a stronger influence on pressure loss than the investigated particle properties within the selected ranges. Therefore, appropriate selection of conveying velocity and pipe diameter is critical for controlling pressure loss and energy consumption in teff pneumatic conveying systems.

The particle properties also influenced pressure drop, although their effects were smaller than those of the system parameters. Within the investigated teff grain property ranges, sphericity from 0.67 to 0.70 was associated with a 50.3% reduction in mean ΔP. Variations in particle density from 1120 to 1381 kg/m³ and particle diameter from 0.68 to 0.72 mm were associated with increases in mean ΔP of 17.9% and 16.6%, respectively. These results demonstrate that variation in teff grain properties, particularly sphericity, should also be considered when evaluating pneumatic conveying performance.

Based on the observed marginal mean changes, the relative influence of the investigated variables was air velocity > pipe diameter ≈ sphericity > particle density > particle diameter. This ordering represents the magnitude of changes observed within the investigated parameter ranges and should not be interpreted as a formal statistical sensitivity ranking.

Overall, the results demonstrate that system parameters, particularly air velocity and pipe diameter, have a greater influence on pressure drop than the investigated particle properties of teff grain. Therefore, careful selection and control of conveying velocity and pipe diameter are essential for reducing pressure loss and energy demand in dilute-phase pneumatic conveying systems. The investigated ranges of particle sphericity, density, and diameter should also be considered in pressure-drop prediction to capture their contribution to conveying performance. These findings provide a quantitative basis for improving the design and operating conditions of teff grain pneumatic conveying systems and offering transferable engineering insights for the dilute-phase transport of similar dry fine bulk materials.

Declarations

Author Contributions: Lemi Demissie Boset: Conceptualization, investigation, data analysis, writing original draft preparation, and writing review and editing.

Data Availability: The datasets generated during and/or analyzed during the current study are available from the corresponding author on reasonable request.

Funding: No funds.

Ethics Approval and Consent to Participate: The cultivated teff (*Eragrostis tef*) grain samples (varieties Felagot, Dagim, and Bishoftu) were obtained with official permission from the National Teff Improvement Program at the Debre Zeit Agricultural Research Center (DZARC/EIAR), Ethiopia. Plant collection and handling complied fully with institutional and national guidelines.

Consent for Publication: Not applicable.

Clinical Trial Number: Not applicable.

Competing Interests: The author declares no competing interests.

References

[1] Abewa, A., Adewale, P. O., & Tadesse, A. (2019). Dimensional and physical characterization of Ethiopian teff cultivars for post-harvest equipment design. Journal of Stored Products Research, 83, 112–120. https://doi.org/10.1016/j.jspr.2019.06.008

[2] Mills, D. (2004). Pneumatic conveying design guide (2nd ed.). Elsevier Butterworth-Heinemann.

[3] McGlinchey, D. (Ed.). (2008). Characterisation of bulk solids. Blackwell Publishing.

[4] Zewdu, A. D., & Solomon, W. K. (2007). Physical and aerodynamic properties of teff (Eragrostis tef) grain. Journal of Food Engineering, 79(1), 334–340. https://doi.org/10.1016/j.jfoodeng.2005.12.037

[5] Boset, L. D. (2025). Numerical sensitivity analysis of particle size, density, and sphericity effects on pressure drop in dilute-phase pneumatic conveying of dry fine bulk materials: A teff grain-based study [Unpublished manuscript]. Department of Mechanical Engineering, Dilla University.

[6] Boset, L. D., Debele, Z. A., & Koroso, A. W. (2025). Determination of pressure drop in positive dilute phase pneumatic teff grain conveyor using experimental CFD-DPM simulation and ANN modeling approach. International Journal of Fluid Power, 26(3), 343–380. https://doi.org/10.13052/ijfp1439-9776.2631

[7] Klinzing, G. E., Rizk, F., Marcus, R. D., & Leung, L. S. (2010). Pneumatic conveying of solids: A theoretical and practical approach (3rd ed.). Springer. https://doi.org/10.1007/978-90-481-3609-4

[8] Rizk, F. (1982). Calculation of pressure drop in horizontal and vertical pneumatic conveying pipelines. Bulk Solids Handling, 2(1), 115–123.

[9] Bradley, M. S. A. (2015). Design of pneumatic conveying systems: A practical guide to system selection and design. Powder Handling & Processing, 27(1), 18–26.

[10] Wypych, P. W. (1999). Pressure drop prediction in dilute-phase pneumatic conveying. Powder Handling & Processing, 11(1), 35–42.

[11] Cabrejos, F. J., & Klinzing, G. E. (1994). Incipient motion of solid particles in horizontal pneumatic conveying. Powder Technology, 79(2), 177–186. https://doi.org/10.1016/0032-5910(94)02816-1

[12] Kaza, S. N., & Jackson, R. (1984). The effect of wall friction on gas-solid flow in horizontal transport lines. Powder Technology, 39(2), 223–233. https://doi.org/10.1016/0032-5910(84)85040-2

[13] Lain, S., & Sommerfeld, M. (2008). Numerical calculation of pneumatic conveying in horizontal pipes accounting for wall roughness and inter-particle collisions. International Journal of Multiphase Flow, 34(6), 554–572. https://doi.org/10.1016/j.ijmultiphaseflow.2007.11.004

[14] Fanning, J. T. (1877). A practical treatise on hydraulic and water-supply engineering. D. Van Nostrand.

[15] Swamee, P. K., & Jain, A. K. (1976). Explicit equations for pipe-friction factor. Journal of the Hydraulics Division, 102(5), 657–664. https://doi.org/10.1061/JYCEAJ.0004542

[16] Weber, M. (1981). Friction limits in pneumatic conveying. Bulk Solids Handling, 1(1), 57–63.

[17] Haider, A., & Levenspiel, O. (1989). Drag coefficient and terminal velocity of spherical and nonspherical particles. Powder Technology, 58(1), 63–70. https://doi.org/10.1016/0032-5910(89)80008-7

[18] Ganser, G. H. (1993). A rational approach to drag prediction of spherical and nonspherical particles. Powder Technology, 77(2), 143–152. https://doi.org/10.1016/0032-5910(93)85005-B

[19] Chen, X. L., & Tomita, Y. (2003). Predictability of velocity and concentration of particles in pneumatic conveying by CFD-DPM model. Powder Technology, 137(3), 173–180. https://doi.org/10.1016/j.powtec.2003.08.050

[20] Hilton, J. E., & Cleary, P. W. (2011). Granular flow in a pneumatic conveying system using DEM-CFD simulation. Chemical Engineering Science, 66(2), 231–240. https://doi.org/10.1016/j.ces.2010.10.029

[21] Kuang, S. B., Li, K. J., & Yu, A. B. (2020). CFD-DEM simulation of gas-solid flow in pneumatic conveying lines: A review. Powder Technology, 363, 678–698. https://doi.org/10.1016/j.powtec.2019.12.029

[22] Tripathi, N. M., & Sharma, A. (2019). CFD simulation of gas-solid flow in horizontal pneumatic conveying pipelines using Eulerian-Lagrangian approach. Advanced Powder Technology, 30(10), 2245–2258. https://doi.org/10.1016/j.apt.2019.07.003

[23] Hölzer, A., & Sommerfeld, M. (2008). New simple correlation formula for the drag coefficient of non-spherical particles. Powder Technology, 184(3), 361–365. https://doi.org/10.1016/j.powtec.2007.08.021

[24] Tsuji, Y., Kawaguchi, T., & Tanaka, T. (1993). Discrete particle simulation of two-dimensional fluidized bed. Powder Technology, 77(1), 79–87. https://doi.org/10.1016/0032-5910(93)85010-7

[25] Huber, N., & Sommerfeld, M. (1998). Modelling and numerical calculation of dilute-phase pneumatic conveying in pipe systems. Powder Technology, 99(1), 90–101. https://doi.org/10.1016/S0301-9322(98)00008-0

[26] Sommerfeld, M. (2003). Analysis of collision effects in particle-laden gas flows. Computers & Fluids, 32(1), 127–142. https://doi.org/10.1016/S0045-7930(01)00099-2

[27] ASAE Standards. (1994). ASAE S352.3: Moisture measurement—Unground grain and seeds. American Society of Agricultural Engineers.

[28] Boset, L. D. (2025). Experimental investigation of minimum fluidization velocity and pressure drop in fluidized bed of teff grain. Journal of Heat and Mass Transfer Research, 12(2), 323–333.

[29] Chambers, A. J., & Marcus, R. D. (1986). Principles of pneumatic conveying. Bulk Solids Handling, 6(3), 437–449.

[30] Gidaspow, D. (1994). Multiphase flow and fluidization: Continuum and kinetic theory descriptions. Academic Press.

[31] Holger, M. (2002). Particle drag coefficients in gas-solid flows: A review. International Journal of Multiphase Flow, 28(8), 1313–1331. https://doi.org/10.1016/S0301-9322(02)00030-2

[32] Konrad, K. (1986). Dense-phase pneumatic conveying: A review. Powder Technology, 49(1), 1–35. https://doi.org/10.1016/0032-5910(86)80002-3

[33] Levy, A., & Mason, D. J. (1998). The effect of a bend on particle cross-section concentration and segregation in pneumatic conveying systems. Powder Technology, 98(2), 95–103. https://doi.org/10.1016/S0032-5910(98)00021-3

[34] Li, H., & Tomita, Y. (2000). A numerical simulation of swirling flow pneumatic conveying in a horizontal pipeline. Particulate Science and Technology, 18(4), 275–291. https://doi.org/10.1080/02726350008906840

[35] Marcus, R. D., Leung, L. S., Klinzing, G. E., & Rizk, F. (1990). Pneumatic conveying systems. Chapman & Hall.

[36] Molerus, O. (1993). Principles of flow and conveying of particulate solids. Chapman & Hall.

[37] O'Dea, S., & Fanning, M. (2018). Pressure drop modeling in pneumatic conveying lines carrying agricultural materials. Biosystems Engineering, 172, 101–115. https://doi.org/10.1016/j.biosystemseng.2018.05.012

[38] Portoghese, F., Berruti, F., & Briens, C. (2008). Continuous online measurement of solids flow rate in pneumatic conveying lines. Powder Technology, 181(2), 169–177. https://doi.org/10.1016/j.powtec.2007.01.009

[39] Rabinovich, E., & Kalman, H. (2011). Threshold velocities for particle pickup and saltation in pneumatic conveying. Powder Technology, 209(1–3), 131–143. https://doi.org/10.1016/j.powtec.2011.02.021

[40] Rhodes, M. (2008). Introduction to particle technology (2nd ed.). John Wiley & Sons.

[41] Yang, W. C. (Ed.). (2003). Handbook of fluidization and fluid-particle systems. CRC Press.

[42] Zenz, F. A., & Othmer, D. F. (1960). Fluidization and fluid-particle systems. Reinhold Publishing Corporation.